

RESEARCH

Open Access



Characteristics and kinetics study of spherical cellulose nanocrystal extracted from cotton cloth waste by acid hydrolysis

Thi Kim Quyen Doan and Kung Yuh Chiang*

Abstract

This work investigated the extraction of spherical cellulose nanocrystal (spherical CNC) from cotton cloth waste (CCW) using sulfuric acid without ultrasound treatment during the hydrolysis process, producing a yield of 31%. The cellulose was first extracted through alkali, decoloring, and hydrochloric acid treatment. Then the cellulose was hydrolyzed using 55 wt% sulfuric acid with various acid to cellulose ratios, including 30:1, 40:1, and 50:1 mL g⁻¹. The resulting CNC was characterized by morphological structure, functional groups, crystalline structure, elemental compositions, thermal degradation kinetic, and zeta potential. The analytical results revealed that the acid to cellulose ratios significantly influenced the properties of CNC obtained. The morphological structure showed that when the acid to cellulose ratio was 30:1 and 40:1 mL g⁻¹, the rod-like CNC was observed with a length of 53 ± 19 nm and 49 ± 13 nm; a width of 6.6 ± 1.3 nm and 4.3 ± 2.0 nm, respectively. However, when the acid to cellulose ratio was further increased to 50:1 mL g⁻¹, the nanocellulose morphology turned to be spherical, with an average diameter of 14.4 nm. Furthermore, spherical CNC exhibited better characteristics consisting of crystallinity index (94.6%) and stable dispersibility with zeta potential value -46.8 mV than rod-like CNC. However, the thermal stability of spherical CNC was slightly lower than that of rod-like CNC. The kinetic results indicated that the activation energy of spherical CNC ranged from 134 to 423 kJ mol⁻¹, which is lower than that (145 to 651 kJ mol⁻¹) of rod-like CNC ranging from. This study showed that the CCW is a potential low-cost cellulose source to manufacture spherical CNC and a good example for developing a circular economy.

Keywords: Cotton cloth waste, Spherical cellulose nanocrystal, Sulfuric acid hydrolysis, Kinetic study, Characterization

1 Introduction

Cellulose nanocrystal (CNC) has recently received more attention due to many unique characteristics, such as biodegradability, high crystallinity, high surface area, high thermal stability, high aspect ratio, a large number of functional groups, and excellent mechanical properties [1, 2]. CNC is known as rod-like CNC with a length of 50–1000 nm and a width of 3–50 nm [3]. Recent studies indicate that spherical CNC is a novel and unique shape,

which exhibits more prominent characteristics than rod-like CNC, such as a uniform morphology with a narrow size distribution [4] and a large surface area compared to rod-like CNC [5]. Hence, spherical CNC has been garnering increasing attention in various fields, such as supercapacitors [6], drug delivery [5], and adsorbent for metal ion removal from wastewater [7].

In published research, spherical CNC can be prepared from various biomass sources, such as cotton waste [8], eucalyptus pulp [9], empty fruit bunch fibers [1], and sago seed shells [10]. Most biomass waste contains low cellulose contents and requires thorough pretreatment before CNC extraction [11]. Meanwhile, cotton

*Correspondence: kychiang@ncu.edu.tw
Graduate Institute of Environmental Engineering, National Central University, Tao-Yuan City 32001, Taiwan



© The Author(s) 2022. **Open Access** This article is licensed under a Creative Commons Attribution 4.0 International License, which permits use, sharing, adaptation, distribution and reproduction in any medium or format, as long as you give appropriate credit to the original author(s) and the source, provide a link to the Creative Commons licence, and indicate if changes were made. The images or other third party material in this article are included in the article's Creative Commons licence, unless indicated otherwise in a credit line to the material. If material is not included in the article's Creative Commons licence and your intended use is not permitted by statutory regulation or exceeds the permitted use, you will need to obtain permission directly from the copyright holder. To view a copy of this licence, visit <http://creativecommons.org/licenses/by/4.0/>.

cloth waste (CCW) has extremely high cellulose content (upward 90%) [12], which corresponds to producing spherical CNC from CCW using lower water and energy consumption as well as input costs [13]. Additionally, CCW accounts for most of the fashion industry waste due to its large share of textile production, with about 25 Mt of cotton fibers being produced annually as a crucial feedstock source to supply the global textile industry [14]. According to the statistics, a tremendous amount of CCW is being dumped in landfills or incineration, which can cause environmental issues such as the emission of foul odor and air pollutants [12]. Therefore, the preparation of spherical CNC from CCW can be an advanced solution for reducing the massive generation of CCW and environmental influences. However, the utilization of CCW for spherical CNC extraction has not gained much attention yet.

Some previous studies have prepared the spherical CNC from cotton waste via a combination of enzymatic hydrolysis and ultrasound treatments [15] and ultrasound treatment during acid hydrolysis [16]. For example, Meyabadi et al. [15] successfully prepared spherical CNC from waste cotton fiber using enzymatic hydrolysis and ultrasound treatments for 175 h at 48 °C. Enzymatic hydrolysis seems to be a green process for CNC preparation. However, enzymatic hydrolysis method produced a low spherical CNC yield of 20% and required a long reaction time [15], causing more energy consumption and higher production cost. Also, enzymatic hydrolysis produced spherical nanocellulose with low dispersibility in solution [17]. The other approach using ultrasound during sulfuric acid hydrolysis can produce spherical CNC with a shorter reaction time than enzymatic hydrolysis. The study of Xiong et al. [16] preparing the spherical CNC from waste cotton fabric via ultrasound treatment during sulfuric acid hydrolysis of 63.5 wt% for 3 h at 44 °C; the result showed that the spherical CNC has a low yield of 21.5% and an average nanoparticle diameter of 35 nm. Although, the ultrasound treatment played a significant role in forming the spherical CNC, the previous research indicated that the environmental impact could be decreased if limiting the use of ultrasonication in CNC preparation [18].

For those limitations, a facile method in spherical CNC production has been conducted using sulfuric acid at appropriate hydrolysis conditions without the assistance of ultrasound during acid hydrolysis. Hafemann et al. [19] used 64 wt% sulfuric acid at 35 °C for 40 min to obtain the spherical CNC with an average yield of 28.1% from royal palm trees. Also, Xu et al. [20] obtained the spherical CNC with a yield of 25.6% from bleached aspen kraft pulp through 64 wt% sulfuric acid at 45 °C for 30 min. This hydrolysis process is simple, effective, and

not time-consuming, but the used acid concentration is high, and the low yield is obtained. The yield is also considered an essential criterion because a high yield is required for any economically feasible process [11]. If the yield enhancement of spherical CNC is required, a low concentration of sulfuric acid is recommended. Thus, if the ultrasound treatment is avoided during acid hydrolysis and the sulfuric acid concentration used is reduced, expecting not only to improve the spherical CNC properties but also reduce the environmental impacts to some extent.

Hence, it is essential to develop the spherical CNC preparation by this alternative approach. However, to the best of our knowledge, there is no published study reporting the spherical CNC preparation from CCW using only sulfuric acid in the hydrolysis process and examined the thermal degradation kinetic of spherical CNC in comparison with rod-like CNC. Also, the acid hydrolysis conditions affecting CNC characteristics from CCW have not been mentioned much in previous literature. Therefore, the objectives of this study were (1) to produce spherical CNC from CCW through sulfuric acid without the assistance of ultrasound during the acid hydrolysis process; (2) to investigate the effects of sulfuric acid to cellulose ratios on the obtained CNC properties; and (3) to investigate thermal decomposition kinetic of the spherical CNC compared to rod-like CNC.

2 Materials and methods

2.1 Materials

CCW was collected from a recycling clothing store in the Zhongli District, Taoyuan City, Taiwan. The CCW included various shirts, pants, and towels with 100% cotton labels. Then the all CCWs were cut into small cloth pieces and mixed them together well. The chemicals used were of analytical grades such as commercial microcrystalline cellulose (CMCC) (Merck's company, Germany), sodium hydroxide (NaOH, Showa-Japan), hydrogen peroxide (H₂O₂, Showa company, Japan), hydrochloric acid (HCl, Fisher chemical, Canada), and sulfuric acid (H₂SO₄, Aencore company, Australia).

2.2 Synthesis of spherical CNC

2.2.1 Microcrystalline cellulose (MCC) extraction procedure from CCW

MCC was extracted from CCW using alkali treatment, decoloring treatment, and hydrochloric acid hydrolysis. First, CCW was cut into small cloth pieces about 1 cm² in size and washed with deionized (DI) water many times to remove dust. The washed CCW pieces were dried in an oven at 105 °C for 24 h. Then CCW was processed through alkali treatment to remove remaining impurities such as hemicellulose, chemical additives, and other

polymeric components. The process followed previous published literature with minor modifications [12]. For alkali treatment, CCW was stirred with a 10 wt% NaOH solution with a ratio of 1:50 (g mL⁻¹) at room temperature and heated up to 80 °C for 3 h. After alkali treatment, the cotton cloth was filtered and rinsed with DI water until the filtrate pH was approximately 10. The dyes were significantly eliminated from alkali treatment, but a small amount of visible dye was still left on the fabric fibers. Therefore, H₂O₂ (1.5 vol%) was used to obliterate the residual dyes. The treated cotton cloth was filtered, washed with DI water until the pH reached neutral, and dried in an oven overnight at 105 °C.

The treated cotton cloth (TCC) was then undergone hydrochloric acid hydrolysis (2.5 N) under mechanical stirring at a ratio of TCC to HCl acid of 1:50 g mL⁻¹ at 80 °C for 60 min. The cellulose suspension was formed as white slurry, filtered, and washed with DI water to remove residual acid until a constant pH (about 6.5–7) was obtained. Finally, the obtained MCC powder was dried at 105 °C for 24 h.

2.2.2 Spherical CNC extraction procedure

Spherical CNC was produced using sulfuric acid hydrolysis of MCC. Sulfuric acid hydrolysis was implemented under constant stirring using 55 wt% H₂SO₄ at 45 °C for 60 min and different acid to cellulose ratios of 30:1, 40:1, and 50:1 mL g⁻¹ (CNC30, CNC40, and CNC50). The hydrolysis process was quenched by adding 5-fold cold DI water. Sulfuric acid residues were removed from the mixture by centrifugation at 5000 rpm for 15 min until the supernatant became turbid. The precipitate was collected and dialyzed (using dialysis tubing with a molecular weight cut-off of 12–14 kDa) against DI water for several days until the neutral pH was achieved. After dialysis, the obtained CNC suspension was homogenized in an ultrasonic bath for 15 min, then kept in the fridge at 4 °C for further characterization.

2.3 Characterization

The obtained samples were characterized by crystalline structure analysis (X-ray diffraction - XRD), morphological examination (scanning electron microscopy-SEM and transmission electron microscopy-TEM), functional group analysis (Fourier-transform infrared spectroscopy-FTIR), zeta potential (ZP) (Zeta sizer ZS90), and thermal degradation (synchronous thermal analyzer). More details about the operation parameters of each characterization are displayed in Supplementary Materials.

The crystallinity index (CrI %) was determined using the XRD peak height method and followed Segal's equation (Eq. (1)) [21].

$$\text{CrI (\%)} = \frac{I_{200} - I_{\text{am}}}{I_{200}} \times 100\% \quad (1)$$

In which I_{200} is the maximum peak intensity of the (200) plane at 2θ value of about 22.6°; I_{am} is minimum intensity between (200) and (110) planes at 2θ value around 18.6°.

The crystalline size was calculated using the Scherrer formula (Eq. (2)), where L_{200} : the crystalline size at the (200) plane, nm; K : Scherrer constant (0.9) [22]; λ : the wavelength of X-ray source (0.15406 nm), B : the half-height width of the peak and θ : the diffraction angle for a chosen diffraction peak.

$$L_{200} = \frac{K \times \lambda}{B \times \cos \theta} \quad (2)$$

2.4 Kinetic study

Thermal stability is directly related to activation energy (E_a) values [23], which can be defined as the minimum amount of energy needed to initiate a chemical process. The E_a for CNC degradation was estimated using the Flynn-Wall-Ozawa (FWO) method at different heating rates of 5, 10, 20, and 40 °C min⁻¹. The FWO expression and the estimated E_a values are shown in Eqs. (3) and (4).

$$\log \beta = \log \left(\frac{A \times E_a}{g(\alpha) \times R} \right) - 2.315 - 0.4567 \left(\frac{E_a}{R \times T} \right) \quad (3)$$

$$E_a = - \left(\frac{R}{0.4567} \right) \frac{\Delta \log \beta}{\Delta \left(\frac{1}{T} \right)} \quad (4)$$

Where β (K min⁻¹) is the heating rate, A is the pre-exponential factor, T (K) is the absolute temperature at conversion (α), R is the ideal gas constant (8.314 J K⁻¹ mol⁻¹), and E_a (kJ mol⁻¹) is the estimated activation energy. E_a values were calculated on the slope ($\Delta \log \beta / \Delta (1/T)$) of the best-adjusted straight line (Eq. (4)).

Conversion α is defined as the change in the reaction extent and is calculated using Eq. (5) with m_o , m_f and m_t (mg) being the initial weight, the final weight, and the weight in the time (t), respectively.

$$\alpha = \frac{m_o - m_t}{m_o - m_f} \quad (5)$$

2.5 Yield and elemental compositions of MCC and CNC

The MCC yield was calculated using the following Eq. (6); where: W_1 and W_2 are weight of CCW and MCC after drying 105 °C for overnight, respectively.

$$\text{MCC yield (\%)} = \left(\frac{W_2}{W_1} \right) \times 100\% \quad (6)$$

The CNC yield was calculated by weighting a 10 mL suspension after oven-drying at 105 °C overnight following Eq. (7) [24].

$$\text{CNC yield (\%)} = \frac{M_2 \times V_1}{M_1 \times V_2} \times 100\% \quad (7)$$

Where M_1 is the initial weight of MCC, M_2 is the weight of CNC after drying at 105 °C, V_1 is the total volume of CNC suspension, and V_2 is the volume of CNC suspension (10 mL) used for oven-drying.

Elemental analysis was used to determine the content of carbon (C), hydrogen (H), sulfur (S) and oxygen (O) using vario Micro cube CHNOS Elemental Analyzer (Elemental Analysensysteme GmbH, Germany).

CNC produced from sulfuric acid hydrolysis appears having sulfate groups on its surface due to esterification of surface hydroxyl groups. The sulfate group density was calculated according to Eq. (8) [25].

$$n_{\text{-OSO}_3^-} = n_S = \frac{S\%}{MW_S} \times 1000 \quad (8)$$

Where $n_{\text{-OSO}_3^-}$ represented the sulfate groups density (mmol g^{-1}); $S\%$ is the percentage of sulfur composition in CNC sample determined using elemental analysis; and MW_S is molecular weight of sulfur (32 g mol^{-1}).

3 Results and discussions

3.1 MCC characterization

3.1.1 MCC yield and elemental compositions

The MCC yield obtained by this study from extraction of CCW was 83%, which was higher than that of the previous reports, which also used hydrochloric acid hydrolysis. For example, MCC from sugarcane bagasse with 55% yield [26], MCC from brown algae with 69.5% yield [27], and MCC from date seeds with 12.5% yield [28]. The high cellulose component in CCW might be responsible for the improvement of the MCC yield. This shows that CCW has outstanding potential in recovering valuable cellulose material. Elemental compositions of samples are shown in Table S1. The percentage of carbon, hydrogen, and oxygen elements were determined in MCC, CMCC, TCC, and the CCW sample. The sulfur and nitrogen contents were not detected in any analyzed samples. The results indicated that all samples contained the typical characteristic of cellulose. As indicated in Table S1, the percentage of elemental compositions of MCC was similar to CMCC, implying successful extraction of MCC from CCW.

3.1.2 Surface characterization by morphological analysis

The macro photographs and SEM images of CCW, TCC, and MCC are shown in Fig. 1. As shown in Fig. 1a and b, the TCC has a bright white color compared to cotton waste which contains many dyed colors, implying the effectiveness of the pretreatment process in removing dyed fabric color. The CCW was observed as a ribbon-like shape with a smooth and uniform surface (Fig. 1d). After the pretreatment process, the fibers of TCC became swollen and appeared on a rough surface (Fig. 1e). The findings indicated that pretreatment could effectively eliminate the impurity components in CCW, such as hemicellulose, wax, and pectin [12]. Then, TCC was subject to hydrochloric acid and resulted in a fine and white powder (Fig. 1c), which were observed as short cylindrical microcrystal morphology (Fig. 1f). This is because hydrolysis reaction formed hydronium ions (H_3O^+) to attack the amorphous regions and broke the β -1,4-glycosidic bonds between two anhydroglucose units from long cellulose chains, resulting in the formation of smaller fragments [27].

3.1.3 Crystalline speciation identification

The XRD spectra of MCC, TCC, CCW, and CMCC are presented in Fig. 2. There are four similar characteristic peaks by all samples at 14.8, 16.6, 22.6, and 34.5°, corresponding to the crystal planes of (1–10), (110), (200), and (004) of cellulose I structure [29]. The XRD diffraction displays that MCC remains intact cellulose I structure during chemical treatments. The result was in agreement with another work reported by Shao et al. [26], who prepared MCC using hydrochloric acid hydrolysis of the corncob. The authors reported that corncob-MCC possessed cellulose I and did not convert it into cellulose II following the chemical treatment process [26]. As shown in Fig. 2, the characteristic peak at around 22.6° was sharper and narrower from CCW to MCC, implying that the obtained MCC grasped the highly ordered crystals and an increase of CrI [30]. This is because hydrochloric acid hydrolysis could remove the amorphous region of CCW and break the glycosidic linkages, resulting in releasing crystallites and increasing the CrI value [31].

The CrI of MCC (95%) obtained by this work is higher than that of oil palm MCC (87%) [32], giant reed MCC (79%) [27] and pomelo peel MCC (41%) [33]. The finding can be related to the low amorphous content of CCW which is easily eliminated by chemical treatments. In addition, the CrI of MCC is found higher than that of CMCC, indicating the extraction process is acceptable and the obtained MCC is a suitable cellulose source for CNC production.

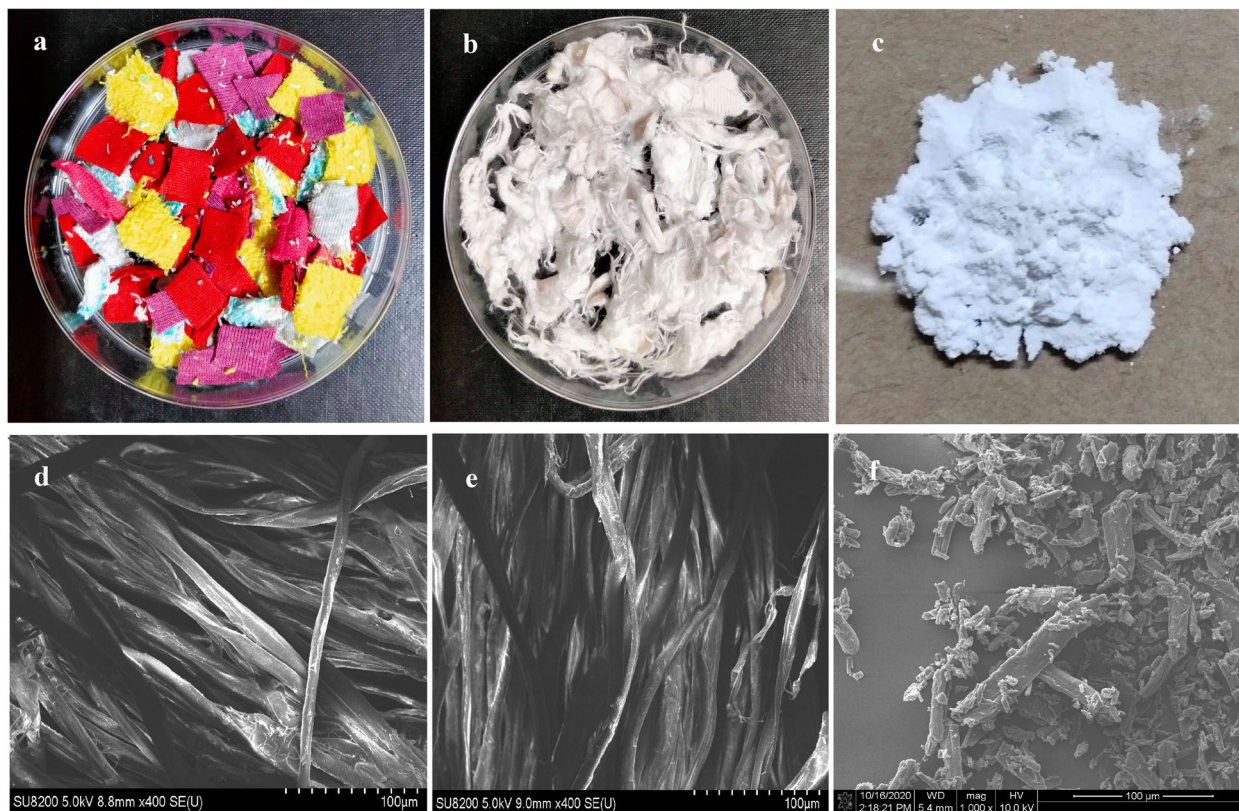


Fig. 1 Photographs of CCW (a); TCC (b); MCC (c) and SEM images of CCW (400X) (d); TCC (400X) (e); MCC (1000X) (f)

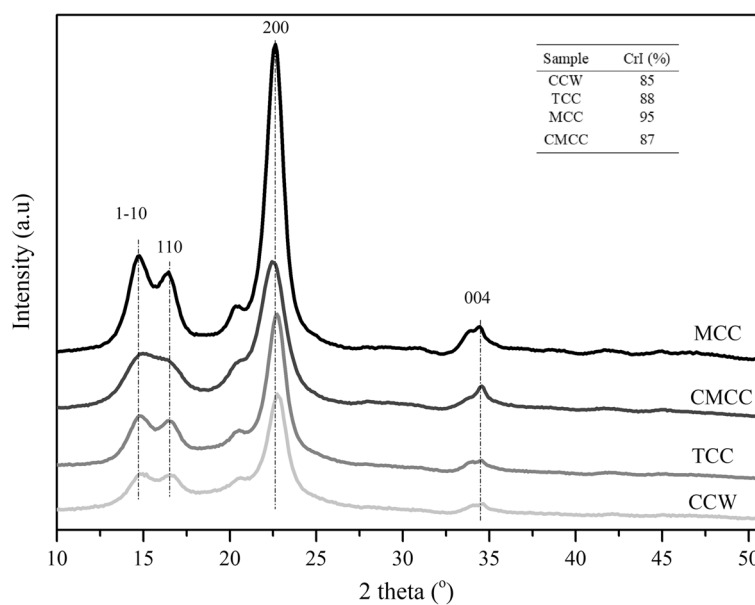


Fig. 2 X-ray diffraction patterns and crystallinity index of MCC, TCC, CCW and CMCC

3.2 Spherical CNC characterization

3.2.1 Acid to cellulose ratio effect on morphological CNC

Figure 3 displays the TEM images of isolated CNC with various acid to cellulose ratios (CNC30, CNC40, and CNC50). Rod-like CNC was observed mainly in CNC30 (Fig. 3a) and CNC40 (Fig. 3b). The average length and width of CNC30 were 53 ± 19 nm and 6.6 ± 1.3 nm, respectively; the average length and width of CNC40 were 49 ± 13 nm and 4.3 ± 2.0 nm, respectively. However, when the acid to cellulose ratio further increased to 50 mL g^{-1} , the CNC morphology turned to be spherical CNC (CNC50), with a small diameter of 14 ± 4 nm (Fig. 3c). Spherical CNC is a spherical or corn-like shaped nanoparticle [34]. These results are consistent with previous study done by Xu et al. [20], in which when the acid to cellulose ratio increased from 9.5 to 10.5 mL g^{-1} , the morphology of CNC became spherical CNC with an average diameter of 3.4 nm. The morphology of spherical CNC obtained in this research is similar to those of spherical CNC reported in other literature [10, 16]. The crystalline structure of spherical CNC is illustrated in HR-TEM results (Fig. 3d). Additionally, selected area diffraction (SAED) patterns and crystalline lattices of spherical CNC were also examined, as shown in Fig. 3c-e. The inset image in Fig. 3c displays the SAED pattern obtained

from the blue circle. The SAED pattern indicated that spherical CNC was a single crystal, and the weak ring pattern was observed due to the appearance of residual amorphous regions. Figure 3e shows crystalline lattice of spherical CNC, which collected from the yellow dashed square in Fig. 3d and produced by an inverse fast fourier transform (inset image in Fig. 3e). As shown in Fig. 3e, the (200) plane was confirmed with lattice-spacing of 3.9 \AA , corresponding to the cellulose I structure [35].

The increase of acid to cellulose ratio investigated by this work is found to be successful in forming spherical CNC. The formation mechanism of different CNC morphologies could be derived from the effects of acid to cellulose ratio related to H_3O^+ produced from the acid hydrolysis process and could attack glycosidic linkages and disintegrate the amorphous regions in the cellulose matrix [19]. Besides, the crystalline regions could retain essentially intact and thus the rod-like CNC was obtained. Furthermore, increasing the acid to cellulose ratio can result in more active hydronium ions in a given amount of cellulose, which tends to hydrolyze the semi-crystalline or amorphous regions faster and more intensely. The result is shorter rods obtained with higher crystallinity and higher-ordered

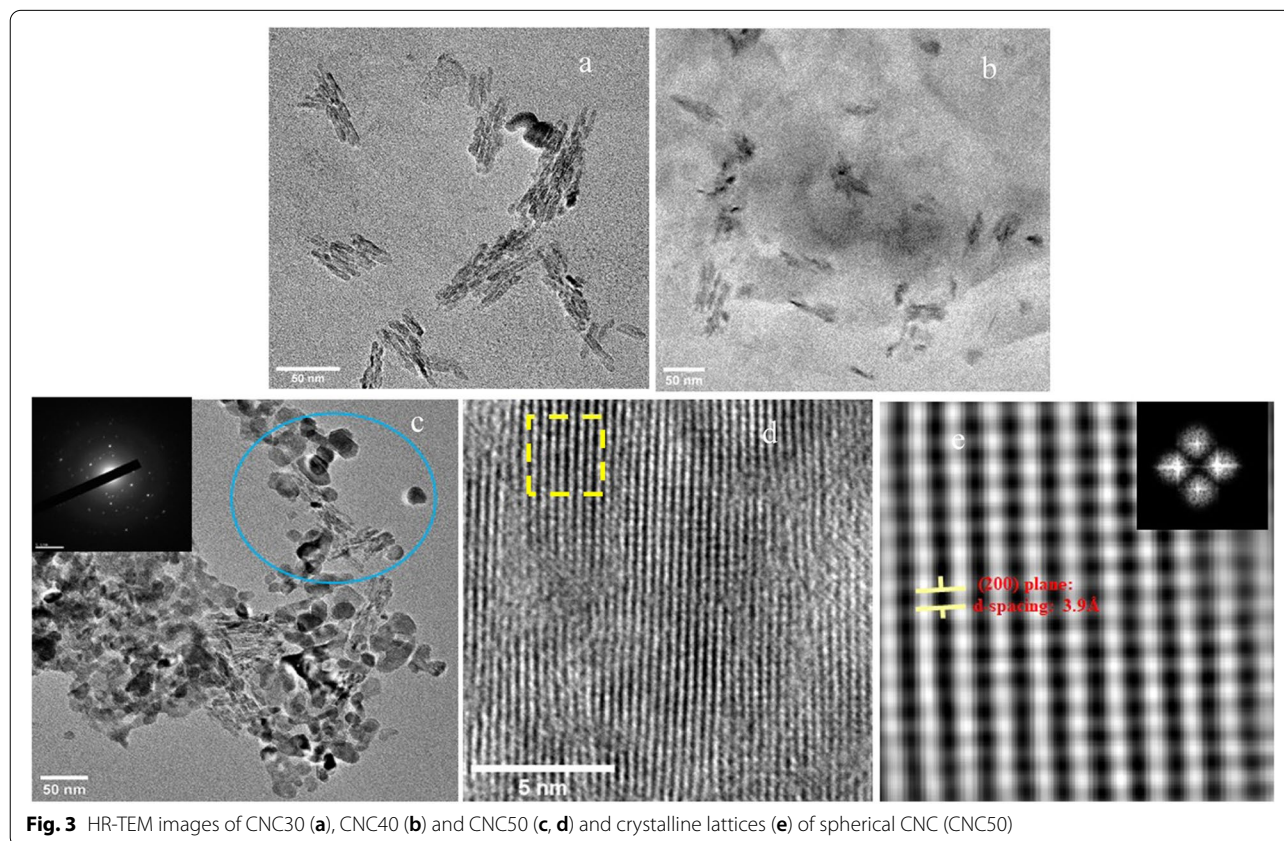


Fig. 3 HR-TEM images of CNC30 (a), CNC40 (b) and CNC50 (c, d) and crystalline lattices (e) of spherical CNC (CNC50)

structure. Then, these shorter rods tend to self-assemble via interfacial hydrogen bond and ultimately form the spherical CNC [10].

Table 1 shows the spherical CNC (CNC50) diameter in this study (14 nm) was comparable to other works using sulfuric acid hydrolysis process; such as spherical CNC obtained from baby diaper waste (10–20 nm) [36] and sago seed shells (10–15 nm) [10]. Furthermore, the nanoparticle diameter of CNC50 is also found much smaller than that of previous researches where the spherical CNC diameter of 30–40 and 40 nm using ultrasound-assisted sulfuric acid hydrolysis from empty fruit bunch fiber [1] and compound enzymatic hydrolysis from eucalyptus pulp [9], respectively. In general, the spherical with

smaller size has remarkable potential in applications, such as drug delivery [5] and cellulose uptake [39].

3.2.2 CNC yield and ZP

The yield, sulfur compositions, and ZP of CNC samples are shown in Table S2. When the acid to cellulose ratio increased from 30:1 to 50:1 mLg⁻¹, the yield of CNC significantly decreased from 52 to 31%. This is because the increase in acid to cellulose ratio means decreasing the amount of cellulose of the hydrolysis process, resulting in decreased CNC yield. Also, the increase of acid to cellulose ratio could promote the degree of cellulose hydrolysis. A similar observation was also reported in the previous study of Xu et al. [20] who indicated that the

Table 1 Comparison of spherical CNC characteristics obtained from various preparation methods and raw materials

Cellulose sources	Preparation method	Preparation conditions				Yield (%)	Crystallinity index (%)	Diameter size (nm)	Ref.
		Acid concentration	Reaction time (h)	Reaction temperature (°C)	Acid: material ratio (mLg ⁻¹)				
CCW	H ₂ SO ₄ acid hydrolysis	55 wt% H ₂ SO ₄	1	45	50:1	31	95	14 ± 4	This study
Baby diaper waste	H ₂ SO ₄ acid hydrolysis	60 wt% H ₂ SO ₄	2	37	9:1	–	–	10–20	[36]
Bleached pine Kraft pulp	H ₂ SO ₄ acid hydrolysis	55 vol% H ₂ SO ₄	0.5	35	25:1	–	85.26	–	[37]
Royal palm tree	H ₂ SO ₄ acid hydrolysis	64 wt% H ₂ SO ₄	0.33	35	20:1	48.8	70.7	–	[19]
Sago seed shells	H ₂ SO ₄ acid hydrolysis	64 wt% H ₂ SO ₄	0.75	45	9:1	–	72	10–15	[10]
Bleached aspen kraft pulp	H ₂ SO ₄ acid hydrolysis	64 wt% H ₂ SO ₄	0.5	45	10.5:1	25.62	84.86	3.38	[20]
Cotton waste	Ultrasound during H ₂ SO ₄ acid hydrolysis	50 vol% H ₂ SO ₄	4.75	–	10:1	–	81.23	50	[8]
Empty fruit bunch fibers	Ultrasound during H ₂ SO ₄ acid hydrolysis	64 wt% H ₂ SO ₄	2	45	–	–	80	30–40	[1]
Waste cotton fabric	Ultrasound during H ₂ SO ₄ acid hydrolysis	63.5 wt% H ₂ SO ₄	3	44	15:1	21.5	84.1	35	[16]
Commercial MCC	Ultrasound blending acid hydrolysis	30 vol% H ₂ SO ₄ , 10 vol% HCl	10	68	25.7:1	–	80	60	[38]
Eucalyptus pulp	Compound enzymatic hydrolysis (cellulase and xylanase with the concentration ratio of 9:1)	500 U mL ⁻¹ of compound enzyme	5	50	10:1	–	91.21	40	[9]
Waste cotton fiber	Enzymatic hydrolysis and sonication treatment	2.3% cellulase enzyme and 5 g L ⁻¹ substrate concentration	175	48	–	20	78.98	70	[15]

–: not available

yield of CNC markedly dropped off when the acid to pulp ratio increased from 8.5:1–10.5:1 mL g⁻¹.

Although the yield of spherical CNC obtained was not as high as expected, this result reflects that the spherical CNC can successfully be prepared by increasing the acid to cellulose ratio without ultrasound during the hydrolysis process. In previous research, the spherical CNC was prepared from cotton-derived cellulose by Xiong et al. [16] using ultrasound during sulfuric acid hydrolysis of waste cotton fabric with 21.5% yield and Meyabadi et al. [15] applying enzymatic hydrolysis and sonication treatment of waste cotton fiber with 20% yield. The limitations of ultrasound treatment and enzymatic hydrolysis in spherical CNC preparation are low yields. Therefore, the spherical CNC from CCW with a yield of 31% obtained in this study can consider as a prospective method for yield improvement of spherical CNC.

The acid to cellulose ratio significantly influenced the sulfate groups on the CNC surface (Table S2). The increase of acid to cellulose ratio could intensify the degree of esterification of the hydroxyl groups and the substitution of these hydroxyl groups by sulfate groups, resulting in grafting more negatively charged sulfate groups on the CNC surface. If nanocellulose has a highly negative charged surface, it can avoid agglomeration and make a stable suspension due to electrostatic repulsion generated between the nanoparticles [10].

The stability of CNC suspension was determined via ZP analysis. ZP is related to the charge present that nanoparticles have. If the absolute ZP value of CNC

suspension is higher than 30 mV, the nanoparticles have enough charge to repulse each other and resist forming agglomeration [40]. Furthermore, the ZP values obtained are proportional to the sulfate group's density (Table S2), and an absolute ZP value of CNC50 (46.8 mV) was higher than that of CNC30 and CNC40. This could suggest that CNC50 with spherical nanocellulose disperses more stable in the aqueous phase than rod-like CNC of CNC30 and CNC40.

Moreover, the obtained ZP of spherical nanocellulose was much higher than compared to that reported by Naduparambath et al. [10] preparing spherical nanocellulose with an absolute ZP value of 37.8 mV using sulfuric acid of sago seed shells. Xu and Chen [17] reported that the spherical CNC obtained from composite enzymolysis of pulp fibers having an absolute ZP value of 28.2 mV. This means that the spherical nanocellulose prepared from sulfuric acid exhibits better dispersion than the enzymatic hydrolysis method. The nanocellulose should generally possess high ZP, which resists the agglomeration and maintains stable dispersibility in the solution.

3.2.3 Functional groups

Figure 4 shows FTIR spectra of CCW, TCC, MCC, CNC30, CNC40, and CNC50. Peaks at 3340 and 2900 cm⁻¹ correspond to O-H stretching vibration and C-H asymmetric stretching vibration [12]. The peaks around 1505 and 1596 cm⁻¹ were assigned to lignin aromatic skeletal vibration C=C bonds. The C-O-C stretching band at 1260 cm⁻¹ could present the lignin ether

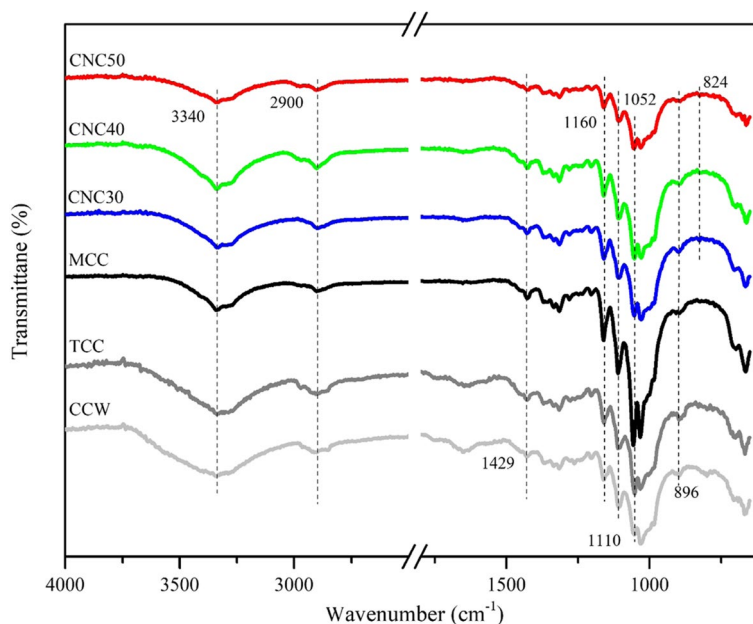


Fig. 4 FTIR of CCW, TCC, MCC and CNC samples

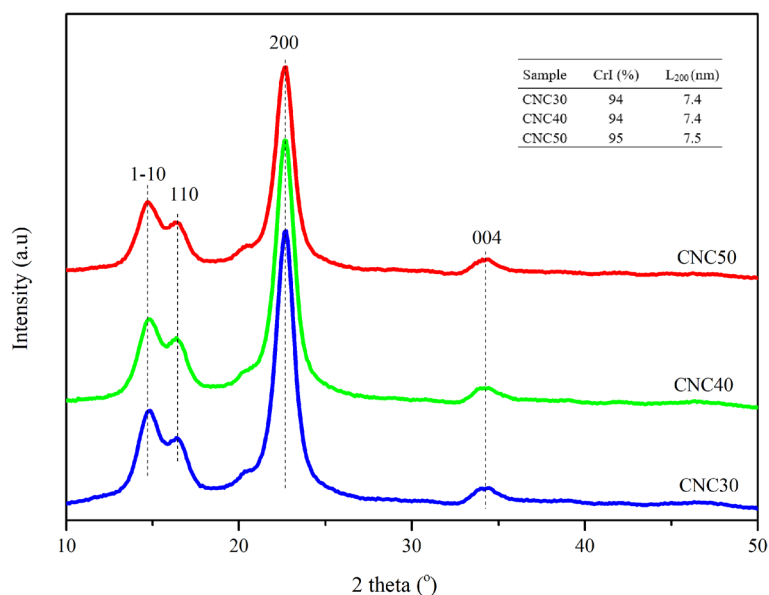


Fig. 5 XRD patterns, crystallinity index and crystallite size of CNC30, CNC40, and CNC50

linkages. However, these bands were not observed in the FTIR analysis, indicating that the lignin composition does not appear in all samples, and the result is consistent with the published works [12, 16]. The peak at 1429 cm^{-1} is related to the bending vibration of $-\text{CH}_2-$. The peaks observed at 1160 and 1110 cm^{-1} are assigned to the bending vibration of C-C and C-O-C within the anhydroglucose ring, respectively [12], indicating that the degradation of cellulose was unlikely to attack glucose rings, whereas the degradation of cellulose should be at β -1,4-glycosidic ring linkage [16]. Some small peaks at 1052 and 896 cm^{-1} correspond to C-O-C pyranose ring vibration and C-H vibration in cellulose, respectively [40, 41]. These bands found in all spectra are related to cellulose I structure, showing that the cellulose components remain during pretreatment and acid hydrolysis. The result agrees with Dungani et al. [42] who extracted CNC from oil palm fronds via sulfuric acid.

Although the cellulose structure did not change, the peak intensity of the obtained cellulose samples markedly changed. The intensity of O-H vibration around 3340 cm^{-1} for MCC, CNC30, CNC40, and CNC50 was lower than that of CCW and TCC. This is because H_3O^+ generated in acid hydrolysis reaction weakened intermolecular hydrogen bonds and broke the cellulose chains, which might be responsible for decreasing hydroxyl groups on the cellulose surface. For CNC samples, the depletion of their surface hydroxyl groups is also due to the contribution of esterification, which replaces these hydroxyl groups with sulfate groups [43]. Observing the intensities of C-O-C (around 1052 cm^{-1}) and C-H

(around 896 cm^{-1}) vibrations in MCC, these intensities were higher than that of CCW and TCC. The result indicated that the non-cellulosic components could be removed effectively in the chemical treatment process and enhance the percentage of cellulose [19]. However, the intensity of these infrared bands in CNC samples showed a noticeable decrease and was proportional to the increase in the acid to cellulose ratio. The findings show that the acid to cellulose ratio affects the magnitude of the hydrolysis reaction on the cellulose structure, resulting in a decrease in the amount of cellulose, consistent with yield results.

3.2.4 CNC crystalline speciation identification

The XRD patterns of rod-like CNC (CNC30 and CNC40) and spherical CNC (CNC50) are shown in Fig. 5. The CrI % and crystallite size are also presented in the inset of Fig. 5. The characteristic peaks were displayed at around 14.7 , 16.6 , 22.7 , and 34.5° , corresponding to the (1–10), (110), (200), and (400) crystal planes, respectively. These planes indicate that rod-like CNC and spherical CNC have the characteristics of cellulose I. The findings are consistent with other researches where diffraction peaks of rod-like CNC and spherical CNC are similar [9, 16, 20]. The results also indicate that the structure characteristics of cellulose I remain intact with increasing ratio of sulfuric acid to cellulose, consistent with FTIR analysis. The CrI of CNC samples did not improve in comparison with that of MCC after sulfuric acid hydrolysis. The findings show that the hydrolysis reaction in the CNC synthesis

not only degrades the amorphous regions but also destroys some crystalline domains [16]. Moreover, the inset (Fig. 5) shows that the CrI values of CNC is stable when the acid to cellulose ratio increased from 30:1 to 40:1 mLg⁻¹. The finding was similar to Xu et al. [20] who indicated that the CrI values of CNC were not significant different as the acid to cellulose ratio increased from 8.5 to 9.5 mLg⁻¹. However, when the ratio was further increased to 50:1 mLg⁻¹, the CrI of CNC50 appeared to increase. The results could be derived from the different morphologies of CNC, since CNC50 with spherical nanocellulose can possess a more organized and crystalline structure which might be responsible for the higher crystallinity index of CNC50 [44].

Crystallite size is another crucial parameter relating to the crystal structure of cellulose. The previous reports mentioned that the increase of crystallite size could result from the increase of CrI [12, 15]. In this study, the CrI of CNC50 is higher than that of CNC30 and CNC40 and consequently larger crystallite size (as shown in inserted table). The crystallite sizes obtained were similar to Maciel et al. [45] preparing CNC samples with a crystallite size of 7.44 nm through sulfuric acid hydrolysis of industrial textile cotton waste. It is worth mentioning that CNC50 with spherical nanocellulose possesses a high CrI, which could improve the mechanical properties (rigidity, tensile strength) of nanocellulose-based composites [46].

The CrI of spherical nanocellulose (CNC50) is approximately 95%, greater than those of results published by others (Table 1). For example, Tong et al. [9] used compound enzymatic hydrolysis to prepare spherical nanocellulose with CrI of 91.2%. The results indicated that the spherical CNC with high CrI could be manufactured from CCW via the adequate sulfuric acid to cellulose ratio.

3.2.5 Thermal properties

Thermal analysis in this study focused on the thermal degradation behavior on CNC samples with different morphologies, including rod-like CNC30 and spherical CNC50. The result of the thermal properties of CNC obtained in Thermogravimetry (TG) and Derivative Thermogravimetry (DTG) curves are displayed in Fig. 6 and Table S3. Thermal analysis of spherical CNC and rod-like CNC was investigated at different heating rates of 5, 10, 20, and 40 °Cmin⁻¹. The TG curves of spherical CNC (Fig. 6a) and rod-like CNC (Fig. 6c) showed an initial slight weight loss of only 2%, found in the temperature range of 100–120 °C due to the evaporation of absorbed water or low molecule compounds.

For spherical CNC, the degradation of cellulose is displayed in two main pyrolysis regions (Fig. 6a and b). The first stage in low temperature of 153–235 °C corresponded to the amorphous degradation regions, which were more accessible and sulfated [37]. The second one

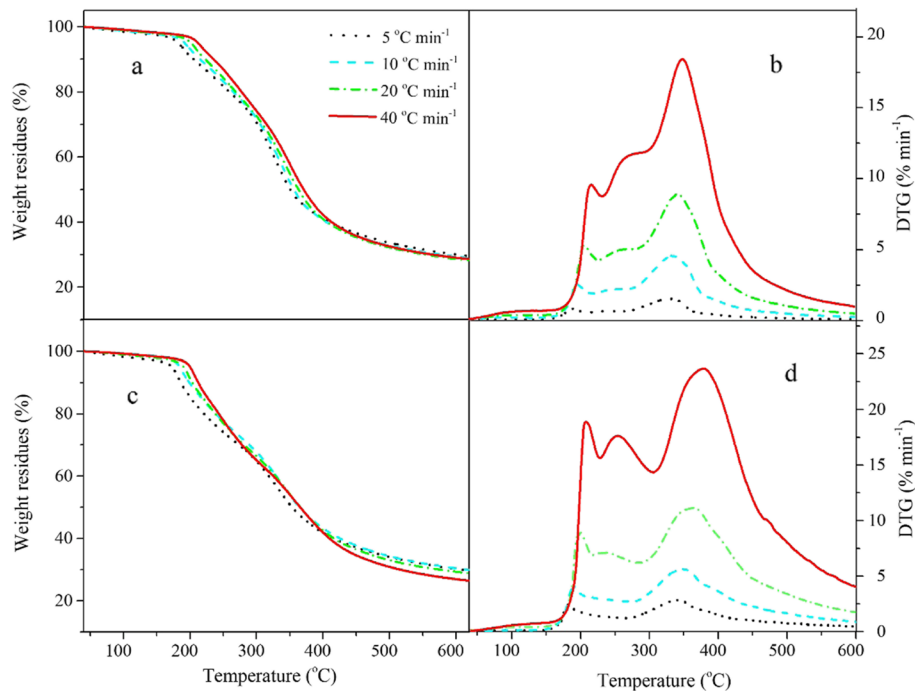


Fig. 6 TG and DTG curves of spherical CNC (a, b) and rod-like CNC (CNC30) (c, d)

at high temperature range of 260–448 °C was attributed to un-sulfated crystalline regions [19]. This degradation process was also observed by Naduparambath et al. [10] who prepared spherical nanocellulose using sulfuric acid hydrolysis of sago seed shells. A similar thermal degradation behavior was observed for rod-like CNC, which also included two degradation stages (Fig. 6c and d). The first and second stages occurred between 150 and 260 °C and 262–450 °C, respectively.

The thermal stability of spherical CNC is expected to be higher than that of rod-like CNC. Onset decomposition temperature (T_{onset}), which is contributed by the thermal stability of a material, was higher for spherical CNC than the rod-like CNC (Table S3). This is because the CrI of spherical CNC was higher than that of rod-like CNC (as shown in XRD results) and consequently higher thermal stability. The results indicated that the CrI contributes positively to the initial thermostability improvement of spherical CNC [47].

However, the spherical CNC exhibited slightly lower thermal stability than the rod-like CNC in the main degradation regions (Table S3). The finding can be related to the presence of sulfate groups on the CNC surface. The previous studies suggested that the higher sulfate groups might be responsible for the lower thermal stability [48]. Also, the E_a of spherical CNC is lower by introducing the negatively charged sulfate groups on the CNC outer surface. Another factor affecting spherical CNC thermal stability could suggest that increasing the acid to cellulose ratio could generate a higher H_3O^+ concentration to access the crystalline domain. As a result, part of the crystalline regions can be dissolved, resulting in its susceptibility to disintegration at high temperatures [49].

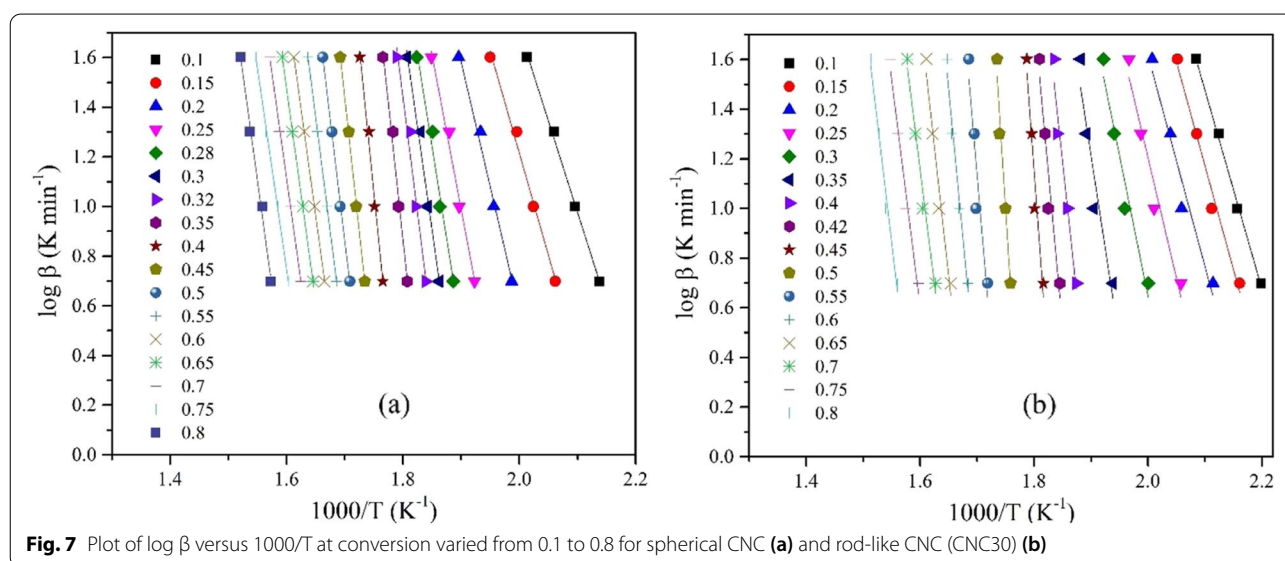
In short, both the CrI and the sulfate group are essential factors for determining the thermal stability of spherical CNC.

3.3 Kinetics results

The E_a is directly associated with the thermal stability of CNC. Hence, the investigation of E_a values could provide a better insight into the thermal degradation of spherical CNC and rod-like CNC. The correlation between $\log \beta$ and $1000/T$ using the FWO method at different conversion (α) values for spherical CNC (CNC50) and rod-like CNC (CNC30) is shown in Fig. 7. The lines illustrated nearly parallel in all samples, confirming approximate E_a values in various conversions [43]. Table S4 indicates a strong correlation with the high value of R^2 and in agreement with the previous research [50].

Both spherical CNC and rod-like CNC (CNC30) showed an increase in E_a values in the conversion range from 0.1 to 0.4, followed by decreased E_a values in the conversion range from 0.5 to 0.8 (Fig. 8). The E_a values in this study were superior to those reported by Henrique et al. [43], who prepared CNC from Kraft pulp using sulfuric acid hydrolysis with the E_a values range from 156 to 269 kJ mol^{-1} . The E_a values of spherical CNC were higher than that of rod-like CNC until conversion closer to 0.35. However, in the conversion ratio from 0.4 to 0.8, the E_a values of spherical CNC were lower than rod-like CNC. These findings demonstrated that the various reactions appeared simultaneously with the CNC degradation [51].

The CrI was considered as an influential factor on CNC's E_a values [43]. Observing in conversion ratio of 0.1 to 0.35, the rod-like CNC has lower E_a values than spherical CNC. This is because the low crystallinity preferred



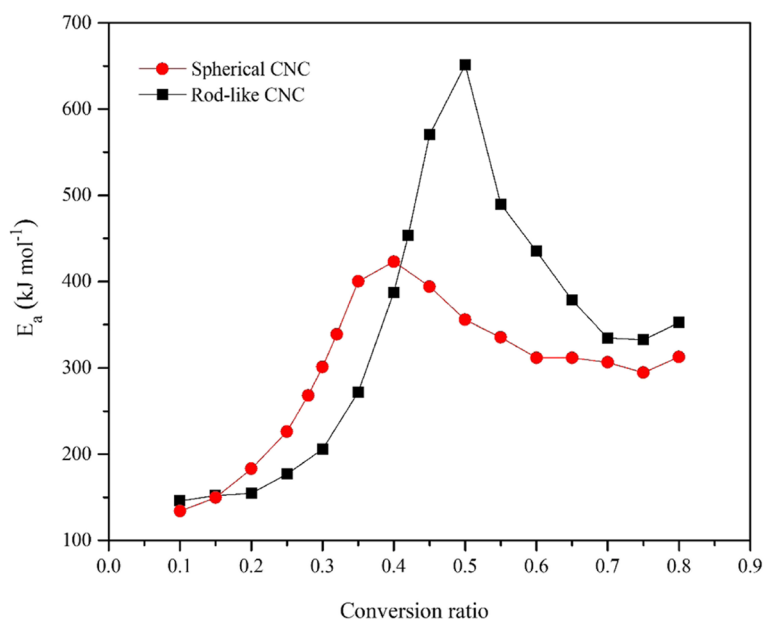


Fig. 8 Activation energy versus conversion ratio for spherical CNC and rod-like CNC (CNC30)

the dehydration reactions, resulting in reduced E_a values [37]. However, after conversion higher than 0.4, the E_a values of spherical CNC were generally lower than that of rod-like CNC. This is because the more negatively charged sulfate groups are introduced into the spherical CNC surface. The results indicated that the more the number of sulfate groups in spherical CNCs, the lesser the E_a needed to be supplied to the degradation process [37].

4 Conclusions

This study successfully extracted the spherical CNC from CCW using chemical treatment and sulfuric acid hydrolysis without ultrasound during the hydrolysis process. The chemical treatment effectively removed the impurity components and amorphous regions in cotton fibers before carrying out the sulfuric acid hydrolysis stage. The yield of spherical CNC (31%) obtained was more efficient than that of spherical CNC mentioned in the literature. The results revealed that the acid to cellulose ratio markedly influences the CNC properties. The morphological structure displayed the rod-like CNC was observed at ratios of 30:1 and 40:1 mLg⁻¹. However, the CNC morphology appeared the spherical shape when the acid to cellulose was further increased 50:1 mLg⁻¹, with a small diameter of 14 nm. The FTIR spectra displayed the cellulose I structure in all samples, but the intensity of cellulose peaks decreased with increasing acid to cellulose ratio. Compared to the XRD and ZP results of rod-like CNC, the spherical CNC possessed a higher crystallinity index (95%) and higher stable dispersion (ZP of -46.8 mV). The

high crystallinity index indicated the extraction process efficiency and facilitated mechanical properties improvement of bio-composite materials. The degradation of CNC samples occurred in two main pyrolysis stages, including the highly sulfated region (150–290 °C) and the unsulfated crystalline region (260–450 °C). The thermal stability of spherical CNC was lower than that of rod-like CNC, which could be derived from the amount of the sulfate groups on the spherical surface and the dissolution of part of the crystalline domains in spherical CNC. The kinetic results indicated that the various reaction occurred simultaneously with the degradation process of CNC. The lower E_a values of spherical CNC could be attributed to higher sulfate groups introduced on its surface. In general, the spherical CNC prepared from CCW would reduce the negative impacts on the natural environment and produce a potential bio-nanomaterial source for biomedical and environmental remediation applications.

Supplementary Information

The online version contains supplementary material available at <https://doi.org/10.1186/s42834-022-00136-9>.

Additional file 1: Materials and methods. The details about the operation parameters of each characterization. **Table S1.** Elemental composition of MCC, CMCC, TCC and CCW. **Table S2.** Yield, sulfur content (S), sulfate groups ($-\text{OSO}_3^-$) and zeta potential (ZP) of the CNC samples. **Table S3.** Thermal degradation parameters of spherical CNC and rod-like CNC obtained at different heating rates. **Table S4.** Activation energy of spherical CNC and rod-like CNC in conversion range of 0.1–0.8 using FWO method

Acknowledgments

The author is very much thankful to the Taiwan Ministry of Science and Technology (MOST) (project No. 109-2221-M-008-023-MY2) for financial support and the Center for Advanced Instrumentation, National Central University, Taiwan, for providing analytical facilities to execute this study.

Authors' contributions

Thi Kim Quyen Doan is the first author responding to collect, analyze data and write the draft manuscript. Prof Kung-Yuh Chiang is the corresponding author who supervised the research and revised the manuscript. All authors have read and approved the final manuscript.

Funding

This research was supported by the Taiwan Ministry of Science and Technology (MOST).

Availability of data and materials

The datasets collected and analyzed during this study mentioned in the submitted article and supplementary materials.

Declarations

Competing interests

The authors declare they have no competing interests.

Received: 9 October 2021 Accepted: 14 April 2022

Published online: 03 May 2022

References

- Azrina ZAZ, Beg MDH, Rosli MY, Ramli R, Junadi N, Alam AKMM. Spherical nanocrystalline cellulose (NCC) from oil palm empty fruit bunch pulp via ultrasound assisted hydrolysis. *Carbohydr Polym* 2017;162:115–20.
- Kim JH, Shim BS, Kim HS, Lee YJ, Min SK, Jang D, et al. Review of nanocellulose for sustainable future materials. *Int J Pr Eng Man-Gt* 2015;2:197–213.
- Kaushik M, Moores A. Review: nanocelluloses as versatile supports for metal nanoparticles and their applications in catalysis. *Green Chem* 2016;18:622–37.
- Ram B, Chauhan GS. New spherical nanocellulose and thiol-based adsorbent for rapid and selective removal of mercuric ions. *Chem Eng J* 2018;331:587–96.
- Zheng DY, Deng YT, Xia Y, Nan YM, Peng MJ, Wang XD, et al. Fabrication and performance of a spherical cellulose nanocrystal-based hydrophobic drug delivery vehicle using rubber wood. *BioResources* 2019;14:7763–74.
- Perez-Madrigal MM, Edo MG, Aleman C. Powering the future: application of cellulose-based materials for supercapacitors. *Green Chem* 2016;18:5930–56.
- Peng S, Meng HC, Ouyang Y, Chang J. Nanoporous magnetic cellulose-chitosan composite microspheres: preparation, characterization, and application for Cu (II) adsorption. *Ind Eng Chem Res* 2014;53:2106–13.
- Pandi N, Sonawane SH, Kishore KA. Synthesis of cellulose nanocrystals (CNCs) from cotton using ultrasound-assisted acid hydrolysis. *Ultrason Sonochem* 2021;70:105353.
- Tong X, Shen WH, Chen XQ, Jia MY, Roux JC. Preparation and mechanism analysis of morphology-controlled cellulose nanocrystals via compound enzymatic hydrolysis of eucalyptus pulp. *J Appl Polym Sci* 2020;137:48407.
- Naduparambath S, Jinita TV, Shaniba V, Sreejith MP, Balan AK, Purushothaman E. Isolation and characterisation of cellulose nanocrystals from sago seed shells. *Carbohydr Polym* 2018;180:13–20.
- Vanderfleet OM, Cranston ED. Production routes to tailor the performance of cellulose nanocrystals. *Nat Rev Mater* 2021;6:124–44.
- Wang ZH, Yao ZJ, Zhou JT, Zhang Y. Reuse of waste cotton cloth for the extraction of cellulose nanocrystals. *Carbohydr Polym* 2017;157:945–52.
- de Figueiredo MCB, de Freitas Rosa M, Ugaya CML, de Souza Filho MDSM, da Silva Braid ACC, de Melo LFL. Life cycle assessment of cellulose nanowhiskers. *J Clean Prod* 2012;35:130–9.
- Shi S, Zhang ML, Ling C, Hou WS, Yan ZF. Extraction and characterization of microcrystalline cellulose from waste cotton fabrics via hydrothermal method. *Waste Manage* 2018;82:139–46.
- Meyabadi TF, Dadashian F, Sadeghi GMM, Asl HEZ. Spherical cellulose nanoparticles preparation from waste cotton using a green method. *Powder Technol* 2014;261:232–40.
- Xiong R, Zhang XX, Tian D, Zhou ZH, Lu CH. Comparing microcrystalline with spherical nanocrystalline cellulose from waste cotton fabrics. *Cellulose* 2012;19:1189–98.
- Xu JT, Chen XQ. Preparation and characterization of spherical cellulose nanocrystals with high purity by the composite enzymolysis of pulp fibers. *Bioresour Technol* 2019;291:121842.
- Li QQ, McGinnis S, Sydnor C, Wong A, Rennecker S. Nanocellulose life cycle assessment. *ACS Sustain Chem Eng* 2013;1:919–28.
- Hafemann E, Battisti R, Marangoni C, Machado RAF. Valorization of royal palm tree agroindustrial waste by isolating cellulose nanocrystals. *Carbohydr Polym* 2019;218:188–98.
- Xu QH, Gao Y, Qin MH, Wu KL, Fu YJ, Zhao J. Nanocrystalline cellulose from aspen kraft pulp and its application in deinked pulp. *Int J Biol Macromol* 2013;60:241–7.
- Segal L, Creely JJ, Martin Jr AE, Conrad CM. An empirical method for estimating the degree of crystallinity of native cellulose using the X-ray diffractometer. *Text Res J* 1959;29:786–94.
- Gumuskaya E, Usta M, Kirci H. The effects of various pulping conditions on crystalline structure of cellulose in cotton linters. *Polym Degrad Stab* 2003;81:559–64.
- Mariano M, Cercena R, Soldi V. Thermal characterization of cellulose nanocrystals isolated from sisal fibers using acid hydrolysis. *Ind Crop Prod* 2016;94:454–62.
- Gong J, Li J, Xu J, Xian ZY, Mo LH. Research on cellulose nanocrystals produced from cellulose sources with various polymorphs. *RSC Adv* 2017;7:33486–93.
- Lin N, Dufresne A. Surface chemistry, morphological analysis and properties of cellulose nanocrystals with gradiented sulfation degrees. *Nanoscale* 2014;6:5384–93.
- Shao XY, Wang J, Liu ZT, Hu N, Liu M, Xu YW. Preparation and characterization of porous microcrystalline cellulose from corncob. *Ind Crop Prod* 2020;151:112457.
- Tarchoun AF, Trache D, Klapotke TM. Microcrystalline cellulose from *Posidonia oceanica* brown algae: extraction and characterization. *Int J Biol Macromol* 2019;138:837–45.
- Abu-Thabit NY, Abu Judeh A, Hakeem AS, Ul-Hamid A, Umar Y, Ahmad A. Isolation and characterization of microcrystalline cellulose from date seeds (*Phoenix dactylifera* L.). *Int J Biol Macromol* 2020;155:730–9.
- Kale RD, Bansal PS, Gorade VG. Extraction of microcrystalline cellulose from cotton sliver and its comparison with commercial microcrystalline cellulose. *J Polym Environ* 2018;26:355–64.
- Kian LK, Saba N, Jawaid M, Fouad H. Characterization of microcrystalline cellulose extracted from olive fiber. *Int J Biol Macromol* 2020;156:347–53.
- Thiangtham S, Runt J, Saito N, Manuspiya H. Fabrication of biocomposite membrane with microcrystalline cellulose (MCC) extracted from sugarcane bagasse by phase inversion method. *Cellulose* 2020;27:1367–84.
- Haafiz MKM, Eichhorn SJ, Hassan A, Jawaid M. Isolation and characterization of microcrystalline cellulose from oil palm biomass residue. *Carbohydr Polym* 2013;93:628–34.
- Liu Y, Liu AL, Ibrahim SA, Yang H, Huang W. Isolation and characterization of microcrystalline cellulose from pomelo peel. *Int J Biol Macromol* 2018;111:717–21.
- Ahmed-Haras MR, Kao N, Ward L. Single-step heterogeneous catalysis production of highly monodisperse spherical nanocrystalline cellulose. *Int J Biol Macromol* 2020;154:246–55.
- Hernandez-Varela J, Chanona-Perez JJ, Benavides HAC, Sodi FC, Vicente-Flores M. Effect of ball milling on cellulose nanoparticles structure obtained from garlic and agave waste. *Carbohydr Polym* 2021;255:117347.
- Trilokesh C, Bavadharani P, Mahapriyadarshini M, Janani R, Uppuluri KB. Recycling baby diaper waste into cellulose and nanocellulose. *Waste Biomass Valor* 2021;12:4299–306.
- Merlini A, Claumann C, Zibetti AW, Coirolo A, Rieg T, Machado RAF. Kinetic study of the thermal decomposition of cellulose nanocrystals with different crystal structures and morphologies. *Ind Eng Chem Res* 2020;59:13428–39.

38. Wang N, Ding E, Cheng RS. Preparation and liquid crystalline properties of spherical cellulose nanocrystals. *Langmuir* 2008;24:5–8.
39. Liebert T, Kostag M, Wotschadlo J, Heinze T. Stable cellulose nanospheres for cellular uptake. *Macromol Biosci* 2011;11:1387–92.
40. Xiao YQ, Liu YN, Wang XJ, Li M, Lei HJ, Xu HD. Cellulose nanocrystals prepared from wheat bran: characterization and cytotoxicity assessment. *Int J Biol Macromol* 2019;140:225–33.
41. Lei WQ, Zhou X, Fang CQ, Li YG, Song YH, Wang CX, et al. New approach to recycle office waste paper: reinforcement for polyurethane with nano cellulose crystals extracted from waste paper. *Waste Manage* 2019;95:59–69.
42. Dungan R, Owolabi AF, Saurabh CK, Khalil HPS, Tahir PM, Hazwan CICM, et al. Preparation and fundamental characterization of cellulose nanocrystal from oil palm fronds biomass. *J Polym Environ* 2017;25:692–700.
43. Henrique MA, Neto WPF, Silverio HA, Martins DF, Gurgel LVA, da Silva Barud H, et al. Kinetic study of the thermal decomposition of cellulose nanocrystals with different polymorphs, cellulose I and II, extracted from different sources and using different types of acids. *Ind Crop Prod* 2015;76:128–40.
44. Kusmono, Listyanda RF, Wildan MW, Ilman MN. Preparation and characterization of cellulose nanocrystal extracted from ramie fibers by sulfuric acid hydrolysis. *Heliyon* 2020;6:e05486.
45. Maciel MMAD, Benini KCCD, Voorwald HJC, Cioffi MOH. Obtainment and characterization of nanocellulose from an unwoven industrial textile cotton waste: effect of acid hydrolysis conditions. *Int J Biol Macromol* 2019;126:496–506.
46. Prasanna NS, Mitra J. Isolation and characterization of cellulose nanocrystals from *Cucumis sativus* peels. *Carbohydr Polym* 2020;247:116706.
47. Poletto M, Pistor V, Zeni M, Zattera AJ. Crystalline properties and decomposition kinetics of cellulose fibers in wood pulp obtained by two pulping processes. *Polym Degrad Stabil* 2011;96:679–85.
48. Martins DF, de Souza AB, Henrique MA, Silverio HA, Neto WPF, Pasquini D. The influence of the cellulose hydrolysis process on the structure of cellulose nanocrystals extracted from capim mombaca (*Panicum maximum*). *Ind Crop Prod* 2015;65:496–505.
49. Mandal A, Chakrabarty D. Isolation of nanocellulose from waste sugarcane bagasse (SCB) and its characterization. *Carbohydr Polym* 2011;86:1291–9.
50. Balogun AO, Lasode OA, McDonald AG. Devolatilisation kinetics and pyrolytic analyses of *Tectona grandis* (teak). *Bioresour Technol* 2014;156:57–62.
51. Mothe CG, de Miranda IC. Study of kinetic parameters of thermal decomposition of bagasse and sugarcane straw using Friedman and Ozawa-Flynn-Wall isoconversional methods. *J Therm Anal Calorim* 2013;113:497–505.

Publisher's Note

Springer Nature remains neutral with regard to jurisdictional claims in published maps and institutional affiliations.

Ready to submit your research? Choose BMC and benefit from:

- fast, convenient online submission
- thorough peer review by experienced researchers in your field
- rapid publication on acceptance
- support for research data, including large and complex data types
- gold Open Access which fosters wider collaboration and increased citations
- maximum visibility for your research: over 100M website views per year

At BMC, research is always in progress.

Learn more biomedcentral.com/submissions

